Chapter 8

Detection of Pathogens Using Microfluidics and Biosensors

Natalia Lopez-Barbosa, Ana Lucia Campaña, Mabel Juliana Noguera, Sergio Leonardo Florez, Miguel Angel Aroca, Juan C. Cruz and Johann F. Osma

Additional information is available at the end of the chapter

http://dx.doi.org/10.5772/intechopen.72443

Abstract

Point-of-care devices technology are a promising way towards the recognition of pathogens in early-stage diagnosis, which is critical for the success of inexpensive treatments as opposed to the high costs of managing the disease. The integration of immunoassays with read out circuitry allows the implementation of diagnostic devices for their use by untrained personnel, without compromising reliability. In the following chapter, three different biosensors based on lab-on-a-chip (LoC) and microfluidic technologies were designed, assembled and tested for pathogen diagnosis. The devices allowed the effective detection of the human papilloma virus, *Mycobacterium tuberculosis* and Chagas parasite in shorter times and with smaller sample volumes than those required by current clinical diagnosis techniques. All devices were benchmarked against commercial techniques in terms of cost and time requirement per test.

Keywords: microfluidics, biosensors, electroimmunosensors

1. Introduction

Diagnostic of pathogenic driven diseases has become a global concern due to the rapid growth of infectious diseases around the world [1]. For decades, pathogen detection has been mainly attained through cell culture, nucleic amplification and enzyme-linked immunoassays, which rely on tedious protocols and are generally time consuming [2]. According to the World Health Organization (WHO), novel technologies for pathogen diagnosis urgently need to address issues regarding affordability, sensitivity, specificity, ease of use, robustness, response time and deliverability to end-users [3]. For this reason, lab-on-a-chip (LoC) and microfluidic

systems, with the inclusion of biosensors, emerge as an attractive alternative due to their low sample volume requirements, rapid response, and ease of integration [4].

The first generation of electrochemical biosensors emerged from the incorporation of immobilized enzymes on conventional electrodes. They were firstly thought for laboratory instruments, but rapidly penetrated into the medical device industry thanks to diagnostic companies [5]. Enzyme-based biosensors exploit the specificity of enzymes towards a particular substrate for sensing purposes [4]. In such devices, immobilized enzymes serve as mediators, easing electron transport from the active site to the electrode [6] and providing a clear signal for substrate recognition. Due to the rather limited availability of substrates, enzyme-based biosensors were rapidly replaced in the medical industry with immunoassays. Antibody-based biosensors rely on the transduction of signals from immobilized antibodies upon binding of specific analytes. This type of biosensors is well accepted in the medical industry for the detection of proteins specific to a particular disease or condition. Electroimmunosensors are antibody-based biosensors that employ electrochemical transducers to obtain an electrical response [7]. The charge transport capacity of the electrodes employed in electroimmunosensors can be monitored via cyclic voltammetry (CV) or as an electrical impedance change via electrochemical impedance spectroscopy (EIS). These two techniques, in conjunction with microfluidics, allow the fabrication of what is usually known as LoC devices.

In the following chapter, we present the design and fabrication of three different systems for detection of human papilloma virus (HPV), tuberculosis and Chagas. Detection of HPV and tuberculosis is effectively achieved by electroimmunosensor LoC technology, while Chagas relies on a microfluidic device for separation and impedance measurement for sensing. The devices are benchmarked against commercial diagnostic devices in terms of ease of use, time of testing and cost.

2. Case of study: HPV

The human papilloma virus (HPV) is a double DNA chain viral pathogen that is sexually transmitted. HPV has been associated with several diseases, such as cervical lesions, condylomas and cervical cancer [8]. Recent studies estimate that between 50 and 80% of sexually active women around the world have been infected with HPV at least once in their lifetime [9]. There are more than 100 different types of HPV strands, some of which are low risk and are generally associated with genital warts. Some other strands, such as HPV 16, are more virulent and may lead to the development of cervical cancer [10]. It is estimated that every year some 500,000 new cases of HPV are diagnosed with condyloma or cervical cancer, which cause around 240,000 deaths in the U.S. [11].

Currently, the preferred assays for diagnosis of HPV infections are hybrid capture (HC) and polymerase chain reaction (PCR) [12]. HC is based on the hybridization of denatured cells with a RNA probe followed by capturing the hybrids via specific binding to antibodies. Signal is amplified by chemiluminescent compound binding through a specific enzyme. This is attained by the conjugation of a secondary antibody with an enzyme that catalyzes the chemiluminescent reaction. Conversely, in PCR, virus detection is performed by the amplification of target DNA aided by DNA polymerases.

Regardless of the accuracy and standardization of laboratory testing, reducing long times of diagnosis and the requirement of specialized personnel, remain as major challenges.

Miniaturization in LoC devices has been widely explored to attain these issues. For instance, Kim et al. [13] developed a microcantilever-based biosensor for the electrical detection of HPV by its conjugation with specific proteins and magnetic beads. Similarly, Huang et al. [14] implemented electrical impedance spectroscopy (EIS) and differential pulse voltammetry on graphene/gold electrodes to detect specific DNA strands of HPV. Although these biosensors have proved to enhance the sensitivity of the detection, Their manufacturing processes are not cost-effective, limiting their accessibility.

Hereby, an antibody-based biosensor with an electronic readout is presented and compared with HC2 and RT-PCR cobas® 4800. The system consists of almost 100 individual test chambers, and was tested with real samples for the detection of HPV.

2.1. Methodology and results

2.1.1. Fabrication of the biomicrosystem

The biomicrosystem was fabricated by self-assembly technique as described in [15]. Briefly, a gold nanolayer was deposited on a poly(methyl methacrylate) (PMMA) substrate via physical evaporation. A second PMMA slide was patterned by laser engraving with 2 mm wells organized in 7 rows and 14 columns. The slide was adhered to the gold-coated PMMA with methylene chloride. Wells were equipped with square holes for electrical connectors. A total of 98 independent biosensors were embedded as shown in **Figure 1**.

Antibody immobilization was attained by placing 4 μL of 97% 4-aminothiolphenol (ATP) (Sigma-Aldrich, USA) in each well. Excess thiols were removed by further ethanol and deionized water rinses. 4 μL of monoclonal antibody (mAb) 5051 was added to each well for immobilization via covalent coupling to the pendant amine group. The biomicrosystem was incubated for 1 h at 37°C and washed with PBS and deionized water.

2.1.2. HPV detection

HPV detection was achieved by EIS and cyclic voltammetry (CV) measurements, and was compared with PCR technique. Samples were obtained from a specialized clinical laboratory

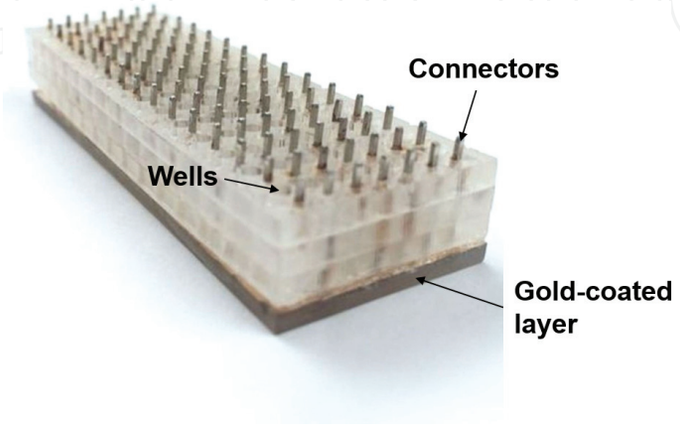

Figure 1. Biomicrosystem for HPV detection.

(PATOLAB, Colombia) from women between 25 and 40 years old. Changes on the impedance were recorded for biomicrosystems with only the gold layer (gold); the gold layer and the thiol (gold-4-ATP); and the gold layer, the thiol and the mAb 5051 (gold-4-ATP-mAb 5051). 10 μL of sample with or without HPV 16 was pipetted in each well and incubated for 1 h at 37°C. Wells were washed with deionized water prior to impedance measurements.

2.1.3. Results

Samples placed in gold-4-ATP-mAb 5051 wells and containing HPV 16 exhibited an impedance change of approximately 40% when compared with initial measurements, while samples without HPV 16 showed an impedance change of less than 5%. Changes in impedance between clean wells and wells of 40 samples with HPV 16 are shown in **Figure 2**.

Impedance changes were significant in wells were the mAb 5051 was immobilized due to its affinity towards HPV 16 proteins.

2.2. Cost analysis

An analytic hierarchy process (AHP) was performed to compare our biomicrosystem with RT-PCR cobas® 4800 and HC2 Test in terms of cost, effectiveness, time required and test analysis. RT-PCR cobas® 4800 allows an automated sample preparation without the need of thawing or mixing, giving results in less than 20 min for up to 94 different samples. HC2 test utilizes *in vitro* nucleic acid hybridization assay with signal amplification towards 13 different HPV specimens.

Cost was considered as the local price of performing one test; effectiveness as the probability of encountering false positives or false negatives; time required as the total time per test; and test analysis as a compounded weigh of the probability of sample contamination, the capacity of

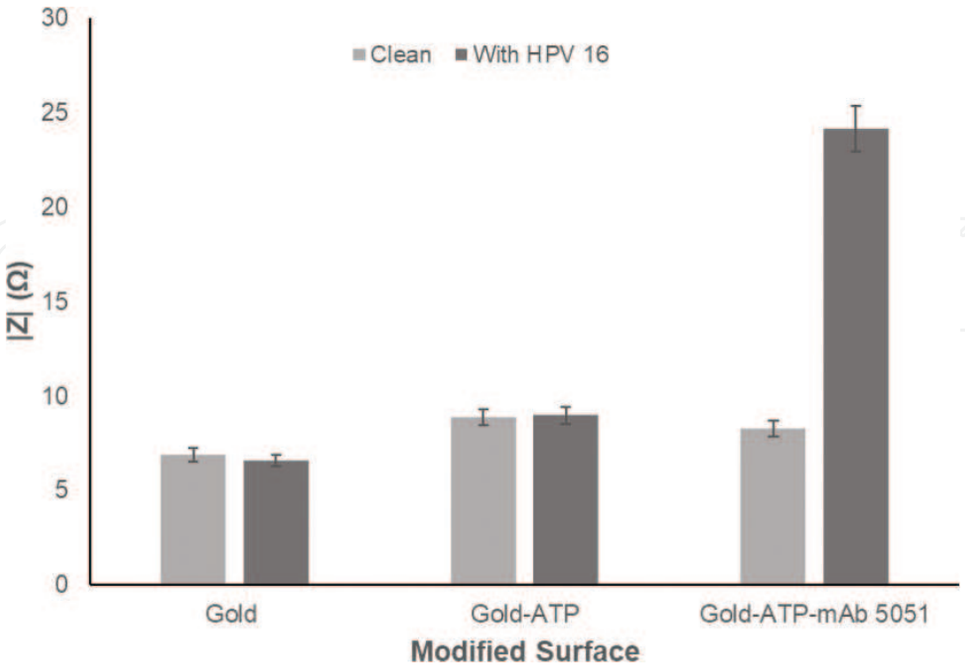

Figure 2. Changes in impedance after exposure to HPV 16 samples.

Test	Cost	Time per test	Contamination probability	Effectiveness with blood in sample	Amount of HPV genotypes per test	Effectivity of the test
Biomicrosystem	Less than commercial tests	2 h	High	High	1	High
RT-PCR cobas 4800	55 USD	2–3 h	None, process is automatized	Medium	14	High
Hybrid Capture 2	63 USD	2–3 h	Low	High	13	High

Table 1. Information used for matrix pairwise comparison.

the test to diagnose with blood in the sample and the number of different HPV genotypes that can be detected per test.

Information for RT-PCR cobra® 4800 and HC2 Test was obtained from three independent specialized laboratories; namely SIPLAS, Quimiolab and Fundacion Santafe de Bogota. Matrix pairwise comparisons based on the scale of Saaty were then conducted on the software Expert Choice 11.5 (ExpertChoice, USA) to evaluate each method [16]. **Table 1** shows the criteria selected and the values for each of the tests.

Global relative weighs of the biomicrosystem, RT-PCR cobas® 4800 and HC2 Test were of 0.343, 0.458 and 0.199, respectively. Our biomicrosystem lags behind the PCR technique due to its inability to detect more than one genotype of HPV. Nonetheless, since the biomicrosystem consists of 98 independent wells, an increase on genotype detection can be achieved by varying the types of antibodies immobilized per well.

3. Case of study: tuberculosis

Tuberculosis (TB) is a disease caused by the pathogenic bacterium *Mycobacterium tuberculosis*. This disease can be effectively controlled by early diagnosis and treatment [17]. Conventional detection technologies include polymerase chain reaction (PCR), enzyme-linked immunosorbent assay (ELISA), and immunochromatographic assay. PCR utilizes oligonucleotides towards a specific gene in *M. tuberculosis* [18]; ELISA is used as a solid phase immunoassay for the detection of an antigen [19]; and immunochromatographic assay is based on the analysis of antigens in a sandwich-based format [20]. These detection technologies exhibit; however, issues regarding long-time of analysis and lack of reliability and sensitivity, which ultimately limit their ability to recognize *M. tuberculosis* [21]. Furthermore, other techniques require various reagents and fluorescent or chemiluminescent labeling for sensing, exhibit low-yields, and may even require further purification steps [22]. Currently, TB is the leading cause of death in people within the most economically productive age-groups and the second deadliest infectious disease in the world [23]. Since diagnosis represents a vital link in the TB control chain, new cost-effective detection platforms are required to achieve quality results in a shorter time span [24].

An alternative route is the use of biosensors, which have attracted significant attention due to their high sensitivity, short analysis time, ease of miniaturization and cost-effectiveness.

Biosensors can be manufactured by the immobilization of biomolecules via self-assembled monolayers (SAMs), which can be generated with the use of thiols, disulfides, silanes, or acids [25]. Among biosensors, immunosensors are devices based on antigen–antibody interaction for the recognition of specific proteins. This interaction is usually transduced into an electrical readable signal [4, 5, 7]. Impedance analysis, a technique based on the measurement of changes in electrical properties of a conductive material [26], is used in this type of biosensors, providing label-free detection and avoiding chemical amplification schemes [27].

In this section, we show the design, manufacturing and testing of biomicrosystems based on printed circuit board (PCB) platforms, with 40 independent electro-immunosensors for the detection of the 6 kDa early secretory antigen target-6 (ESAT-6), which is an immunodominant secreted protein involved in the virulence of *M. tuberculosis* [28]. Sensors were integrated into a microfluidic system that allows the use of a minimum volume of sample per test. Human serum albumin (HSA) was employed as a negative control. Each electro-immunosensor was comprised of a gold nanolayer with an immobilized polyclonal antibody (pAb) attached by a thiol-based SAM. Without the need of intrusive or destructive methods, it was possible to detect probe-target interactions and verify all manufacturing stages of the biomicrosystem via impedance analysis at different frequency ranges [29].

3.1. Materials and methods

3.1.1. PCB design and manufacture

Each biomicrosystem was mounted on a double-layer FR-4 PCB of 142 × 48.7 mm with 2 oz. thickness of copper. Electrodes were patterned on the top layer while interconnection tracks were placed on the bottom layer with CadSoft Eagle Professional 7.4.0. The PCB bottom surface was laminated with antisolder and the top layer was left uncovered for further material deposition. The PCB electrical conductivity was verified through PeakTech 3725 multifunction digital tester (PeakTech, Ahrensburg, Germany).

3.1.2. Lift off and gold deposition

A uniform gold nanolayer was physically evaporated to form the electrodes at the top layer of the board. Briefly, the substrate top surface was laminated with a dry photosensitive film (LAMINAR® E9200) in the RLM 419P (Bungard Elektronik, Windeck, Germany) laminator. The substrate was exposed to UV light to promote free-radical polymerization. The laminated substrate was subjected to a developing process and a uniform gold nanolayer was physically evaporated on the laminated substrate through physical vapor deposition (PVD) with thermal evaporator Edwards Auto 306 (Moorfield Nanotechnology Limited, Cheshire, UK). A 3 A current, vacuum pressure of 4×10^{-5} mbar and an evaporation rate of 0.12 nm/s were used over a tungsten slide for 100 mg gold evaporation. Finally, photoresist sacrificial layer was removed with stripper (Bungard Elektronik, Windeck, Germany), obtaining an 80 nm gold nanolayer on 35 μm copper surfaces. The electrical conductivity of individual electrodes on the board of each biomicrosystem was verified using a PeakTech 3725 multifunction digital tester (PeakTech, Ahrensburg, Germany).

3.1.3. Biomicrosystem development

A 121 × 20.8 mm PMMA slide with 2 mm wells organized in two rows and 20 columns was adhered to the top of the PCB top layer using TESA® 4965 double-sided tape and subsequently fixed with screws (**Figure 3a**), miming a well plate with individual wells for each electrode. Reagents were deposited inside each well for the biosensor fabrication (**Figure 3b**) and electrical connectors were placed between each well for electrical measurements (**Figure 3c**). Three biomicrosystems were fabricated and tested in different batches, each biomicrosystem containing 40 independent electro-immunosensors, which were individually measured for each batch (**Figure 3d**) to assure the reproducibility and repeatability of the manufacturing process. A total of 120 electro-immunosensors were tested.

3.1.4. Reagents immobilization

SAM were produced in each well following the procedure in [15]. Shortly, 10 μL of 20 mM 4-aminothiophenol (4-ATP) solution were added as cross-linkers in each well and left at room temperature for 4 h. To remove excess of thiols, wells were washed with ethanol and deionized water. 10 μL of 100 μg/mL pAb 45073 solution were added into each well. The system was stored at 4°C overnight. PBS and deionized water were used to remove excess biomolecules.

3.1.5. Immobilization tests

Impedance measurements of each well of the electro-immunosensor were according to the diagram shown in **Figure 3d** and using an impedance analyzer (Agilent 4294A) at a frequency

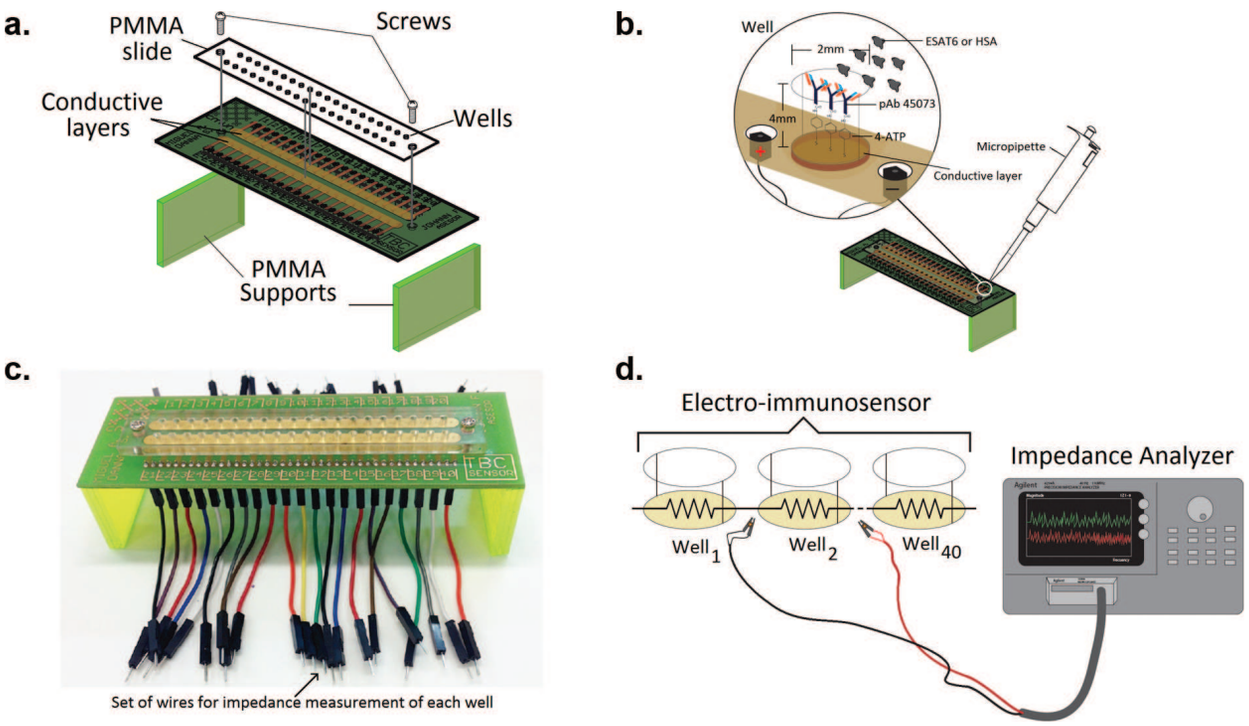

Figure 3. (**a**) Schematic representation of the biomicrosystem, (**b**) illustration of the self-assembly process for each well, (**c**) actual image of the fabricated biomicrosystem, and (**d**) equivalent measurement circuit of the biomicrosystem.

range from 40 to 120 Hz, 120 to 200 Hz and 200 to 280 Hz. Frequencies were selected as reported in [15]. Sensors were manufactured in three main stages, first a gold nanolayer (Au), followed by a gold nanolayer with a SAM of 4-ATP (Au + ATP), and finally a gold nanolayer with a SAM of 4-ATP and pAb 45073 (Au + ATP + pA). Eight replicates of the impedance measurements were collected at each stage for the specific frequencies above. Impedance analysis was also performed for analyte recognition in the presence of both 0.5 μg/mL of ESAT6 (Au + ATP + pA-ESAT6) (positive control) and HSA (Au + ATP + pA-HSA) (negative control). After analyte deposition, wells remained at room temperature and under static conditions for 1 h prior to electrical measurements.

3.2. Results

3.2.1. Immobilization testing by impedance analysis

The average impedance magnitude of the three manufacturing stages of the sensors (Au, Au + ATP, Au + ATP + pA) was determined by its response to an AC current as a function of frequency [30]. To determine the variation of the copper with gold evaporated prior to the immobilization (conductive layer), 40 individual wells of three biomicrosystems were measured by impedance analysis at different frequency ranges. The mean value of the 120 wells was 0.1588 Ω with a standard deviation of 0.0142, 0.1591 Ω with a standard deviation of 0.0142, and 0.1584 Ω with a standard deviation of 0.0102 Ω, for ranges 40–120 Hz, 120–200 Hz and 200–280 Hz, respectively. This suggested small variance and good reproducibility of the manufacturing processes of all wells regardless of the fabrication batch. The largest significant differences within immobilization stages were observed for 40 and 120 Hz (**Figure 4**, **Table 2**).

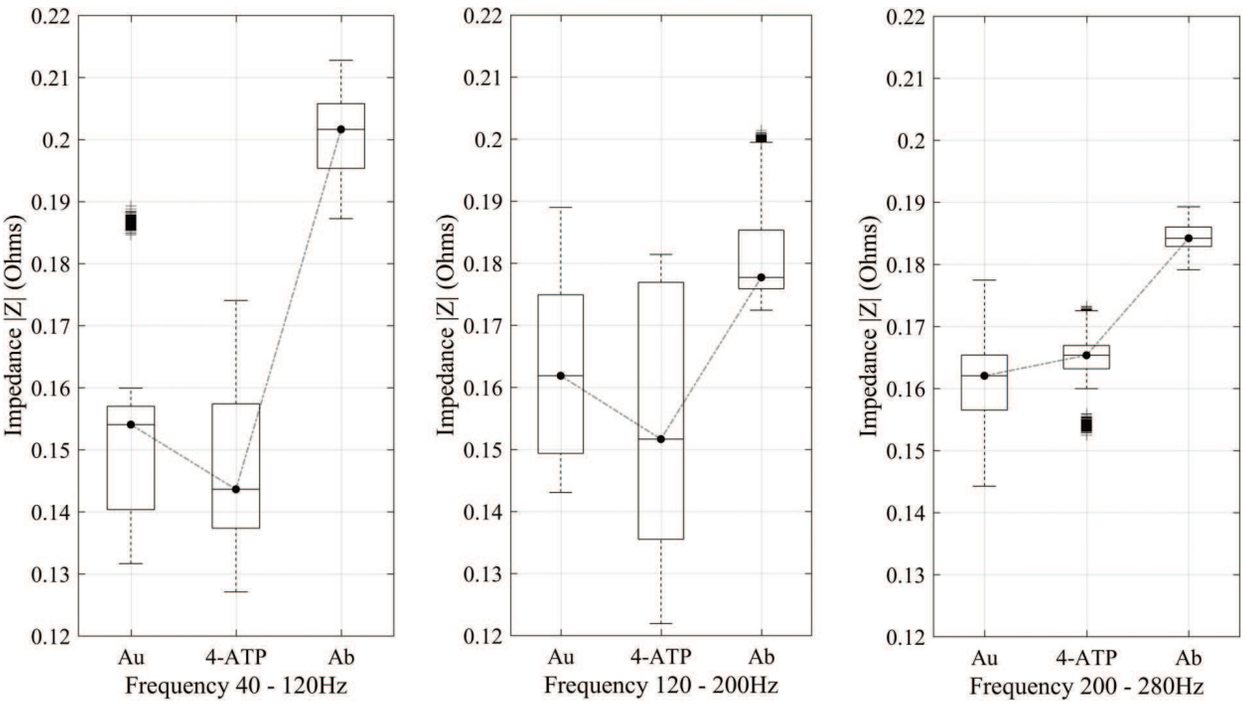

Figure 4. Analysis of impedance variation for the three main manufacturing stages. (**a**) Impedance magnitude at 40–120 Hz, (**b**) impedance magnitude at 120–200 Hz, and (**c**) impedance magnitude at 200–280 Hz.

Frequencies	|Z| Au		|Z| 4-ATP		|Z| Ab	
	Average (μ) Au	Standard Deviation (σ) Au	Average (μ) 4-ATP	Standard Deviation (σ) 4-ATP	Average (μ) Ab	Standard Deviation (σ) Ab
40	0.1526	0.0167	0.1466	0.0145	0.1986	0.0070
50	0.1523	0.0165	0.1482	0.0142	0.1997	0.0067
60	0.1517	0.0169	0.1472	0.0141	0.2004	0.0065
70	0.1523	0.0167	0.1475	0.0144	0.1996	0.0065
80	0.1530	0.0160	0.1473	0.0139	0.2009	0.0068
90	0.1528	0.0159	0.1470	0.0144	0.2018	0.0071
100	0.1530	0.0165	0.1471	0.0142	0.2016	0.0068
110	0.1525	0.0159	0.1470	0.0143	0.2003	0.0070
120	0.1532	0.0166	0.1472	0.0140	0.2009	0.0070
130	0.1629	0.0159	0.1542	0.0220	0.1819	0.0083
140	0.1627	0.0156	0.1540	0.0213	0.1821	0.0084
150	0.1629	0.0158	0.1540	0.0216	0.1814	0.0083
160	0.1624	0.0157	0.1549	0.0219	0.1815	0.0084
170	0.1624	0.0159	0.1534	0.0216	0.1807	0.0081
180	0.1627	0.0155	0.1535	0.0216	0.1812	0.0085
190	0.1624	0.0154	0.1535	0.0218	0.1809	0.0082
200	0.1629	0.0155	0.1537	0.0216	0.1805	0.0084
210	0.1612	0.0088	0.1653	0.0052	0.1846	0.0022
220	0.1614	0.0089	0.1646	0.0052	0.1844	0.0020
230	0.1605	0.0088	0.1655	0.0051	0.1850	0.0021
240	0.1605	0.0089	0.1644	0.0051	0.1839	0.0019
250	0.1619	0.0087	0.1649	0.0051	0.1846	0.0021
260	0.1613	0.0089	0.1646	0.0052	0.1838	0.0023
270	0.1611	0.0090	0.1646	0.0049	0.1845	0.0019
280	0.1610	0.0087	0.1654	0.0047	0.1843	0.0022

Table 2. Impedance magnitude values (mean and standard deviation) of the manufacturing stages at 40–280 Hz.

In this range, there is a non-significant variation of impedance (−3.81%) between the first two manufacturing stages, Au and Au + ATP. Nonetheless, a 31.21% of impedance variation between Au and Au + ATP + pA was measured. Also, impedance measurements between the first two manufacturing stages varied −5.51% and 2.16%, from 120 to 200 Hz and from 200 to 280 Hz, respectively. Similarly, variations of 11.4 and 14.37% between Au and Au + ATP + pA were detected at frequencies ranges of 120 to 200 Hz and 200 to 280 Hz, respectively. Finally, there was a correspondence between the impedance value of the last immobilization step and negative controls, which was 0.20 Ω [29].

3.2.2. Detection of protein ESAT6

Impedance analysis was used to verify the detection of ESAT6 as means of *M. tuberculosis* diagnosis. 0.5 μg/mL ESAT-6 were used as a positive control and 0.5 μg/mL HSA as a negative control, and their detection was compared to the dot blot assay. **Figure 5** and **Table 3** show that the frequency range from 40 Hz to 120 Hz has the largest significant variation in impedance among all investigated ranges. **Figure 5c** and **d** shows significant changes in other frequency ranges (120–200 Hz and 200–280 Hz). Between 40 and 120 Hz, the detection of the *M. tuberculosis* protein has an impedance increase of 171% compared to the impedance measured for the negative control (HSA), which showed a negligible impedance variation. No overlapping values between the negative and the positive control were identified. All the results of the negative controls were under 0.20 Ω while impedance values for the positive controls were above 0.54 Ω. This defined an interval where protein detection is not attainable.

3.3. Analytic hierarchy process (AHP) for comparison of the biomicrosystem with traditional detection techniques

AHP was utilized to study the viability of the electro-immunosensor compared with traditional TB diagnostic techniques (Xpert MTB/RIF, culture, and smear test). Expert Choice 11.5® software was used to perform matrix pairwise comparisons in light of the scale of Saaty [16]. **Table 4** summarizes the required parameters for the pairwise comparison matrix. This weighed analysis compared cost, effectiveness, time, and test analysis for each diagnostic platform. This program assigns a weight to each of the alternatives relative to the criteria. The total weight is distributed among the diagnostic alternatives, which were the electro-immunosensor, Xpert MTB/RIF, culture and smear test. **Table 5** shows the results obtained [29].

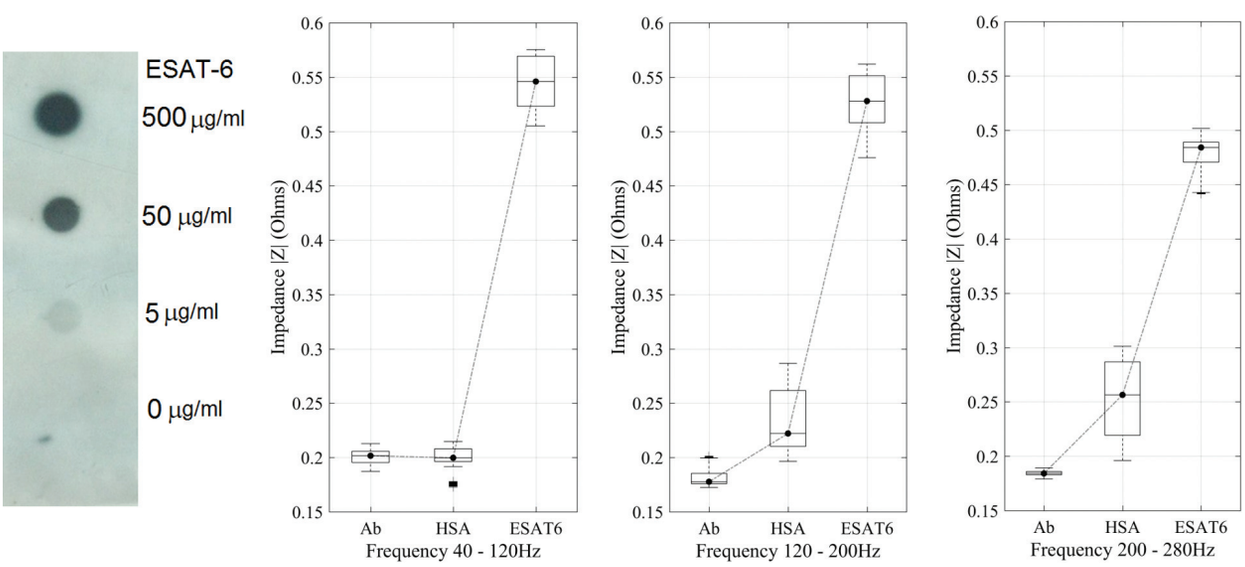

Figure 5. (**a**) Detection limit for the dot blot assay compared to the electro-immunosensor. (**b**, **c**, **d**) Analysis of impedance variation for 0.5 μg/mL of analyte. (**b**) Impedance magnitude at 40–120 Hz, (**c**) impedance magnitude at 120–200 Hz, and (**d**) impedance magnitude at 200–280 Hz.

Frequencies	|Z| Ab		|Z| HAS		|Z| ESAT6	
	Average (μ) Ab	Standard Deviation (σ) Ab	Average (μ) HSA	Standard Deviation (σ) HSA	Average (μ) ESAT6	Standard Deviation (σ) ESAT6
40	0.1986	0.0070	0.2016	0.0114	0.5462	0.0264
50	0.1997	0.0067	0.1986	0.0116	0.5440	0.0254
60	0.2004	0.0065	0.1986	0.0118	0.5439	0.0260
70	0.1996	0.0065	0.2000	0.0112	0.5446	0.0260
80	0.2009	0.0068	0.1991	0.0114	0.5443	0.0259
90	0.2018	0.0071	0.1988	0.0109	0.5440	0.0256
100	0.2016	0.0068	0.1988	0.0114	0.5438	0.0260
110	0.2003	0.0070	0.1986	0.0113	0.5437	0.0260
120	0.2009	0.0070	0.1986	0.0114	0.5434	0.0263
130	0.1819	0.0083	0.2340	0.0320	0.5266	0.0292
140	0.1821	0.0084	0.2338	0.0317	0.5267	0.0288
150	0.1814	0.0083	0.2337	0.0318	0.5264	0.0292
160	0.1815	0.0084	0.2338	0.0316	0.5264	0.0294
170	0.1807	0.0081	0.2336	0.0315	0.5262	0.0295
180	0.1812	0.0085	0.2337	0.0319	0.5262	0.0296
190	0.1809	0.0082	0.2340	0.0315	0.5260	0.0294
200	0.1805	0.0084	0.2336	0.0318	0.5266	0.0291
210	0.1846	0.0022	0.2540	0.0373	0.4820	0.0153
220	0.1844	0.0020	0.2537	0.0372	0.4805	0.0156
230	0.1850	0.0021	0.2532	0.0371	0.4798	0.0154
240	0.1839	0.0019	0.2527	0.0372	0.4786	0.0159
250	0.1846	0.0021	0.2522	0.0370	0.4779	0.0163
260	0.1838	0.0023	0.2519	0.0368	0.4784	0.0169
270	0.1845	0.0019	0.2515	0.0371	0.4789	0.0177
280	0.1843	0.0022	0.2513	0.0367	0.4826	0.0144

Table 3. Impedance magnitude values (mean and standard deviation) of different analytes at 40–280 Hz.

The AHP analysis confirmed that the designed electro-immunosensor is a superior alternative for detection compared with traditional TB diagnostic techniques. For instance, it requires a shorter time of analysis per test and allows high throughput screening (a single device handles 40 independent replicas), and even the identification of different *M. tuberculosis* epitopes by varying the bio-recognition probe in each well. Despite these advantages, the electro-immunosensor is not the preferred choice locally mainly due to its prohibitive price (attributed to the cost of required bioreagents) and the untested effectiveness in clinical contexts.

Test	Cost	Time of analysis	Probability of contamination	Difficulty of analysis with blood in sample	Test effectiveness
TBC biosensor	7 USD (without labor and overhead)	1 h	Low: although it is a manual process, there are mechanical barriers to avoid filtration between wells	It is based on antigen-body recognition, so bleeding is not supposed to affect the results	Results confirm that reliable data is obtained with the biosensor
Xpert MTB/RIF	98.10 USD	2 h	None: completely automated	There is no interference after the pretreatment	High sensitivity, specificity and reproducibility. Avoid false positive/negative results
Culture (MGIT)	36.56 USD	1 month	Medium: microbial growth can be affected by accompanying microbiota	Bleeding does not affect the results	Reliability between 70 and 90%
Smear microscopy test	4.07 USD	More than 1 day	None: it is a fast and direct method	There is no interference after the pretreatment	It depends on the sample and technician. Reliability can vary between 22 and 80%

Table 4. Criteria for the establishment of the pairwise comparison matrix for the diagnostic techniques for *M. tuberculosis*.

	Electro-immunosensor (%)	Xpert MTB/RIF (%)	Culture (%)	Smear test (%)
Retail price	31.0	4.3	11.3	53.4
Analysis of tests	35.6	15.8	28.1	20.5
Effectiveness	10.6	14.4	54.3	20.8
Time of test	50.2	29.0	4.1	16.7
Global weights	32.5	16.7	22.5	28.3

Table 5. Local weights for each diagnostic platform.

4. Case of study: Chagas

Development of methods that can facilitate low-cost diagnosis of infectious and particularly neglected tropical diseases has been widely studied in the last few decades. In this section, we outline the design, fabrication and evaluation of a portable system for the detection of Chagas Disease during the Acute phase of the disease, called Chagas Biosense, as an alternative to perform a quick, on-site, and low-cost diagnosis. Furthermore, we describe its potential impact on alleviating the economic burden on the healthcare system by improving rural diagnostics of Chagas in developing and tropical countries.

4.1. Theoretical framework

4.1.1. Fundamentals of Chagas disease

The World Health Organization (WHO) classifies 17 major parasitic and bacterial infections as neglected tropical diseases (NTDs) [31]. NTDs are characterized by affecting vulnerable

populations (where healthcare systems are generally inefficient), and their survival under tropical and subtropical conditions [32]. American trypanosomiasis, better known as Chagas disease, is one of the most common NTDs in the world, which is caused by the parasite *Trypanosoma cruzi*. Recent estimates indicated that between 6 and 7 million people are infected worldwide [32].

Chagas is a vector-born disease transmitted by triatomine insects. This hematophagous insect of the *Reduviidae* family, transmits the disease while feeding [33]. The infection starts with the movement of the parasite from the insect feces into human blood streams. From this point, the disease will develop in two consecutive phases. First, the Acute phase, characterized for a high number of parasites present in the bloodstream, lasting for about 4 to 8 weeks and showing very mild or non-existent symptoms [34]. Second, the Chronic phase, where the immune system of individuals is compromised and some organs are infested with the *Trypanosoma cruzi* [34]. In fact, when the patient reaches the Chronic phase, the parasite invades the digestive system and the heart tissues, which can cause damages that will be evidenced up to 20 years after the infection [35]. Most commonly, patients will manifest progressive heart damage, which may eventually require a heart transplant [34, 35].

Nowadays, treatments to the disease include benznidazole and Nifurtimox. Both treatments are 100% effective in killing the parasite and treating the disease if they are used at the beginning of the Acute phase. The efficacy of both treatments decreases as the infection progresses [32].

4.1.2. Current diagnosis methods

Diagnosis of Chagas Disease is carried out by observation of the parasite in a blood sample by means of microscopy methods, such as blood cultures, xenodiagnoses and thick drop, among others. However, these methods only work during the Acute phase of the disease, due to the important number of parasites in the bloodstream [9]. Diagnosis in the Chronic phase is determined based on the medical history of the patient, and only if the patient has lived in an endemic area. Thus, diagnosis during this phase relies on laboratory tests based on antibodies specific for the disease, ELISA tests, and quick tests such as Chagas STAT-PAK® [36]. **Table 6** summarizes the main characteristics of most popular diagnosis tests, as well as our system.

4.1.3. Chagas biosense concept

An effective detection method of Chagas Disease relies on the basic understanding of the parasite behavior inside the human circulatory system. The parasite in its infectious stage (*metacyclic trypomastigote*) reaches the circulatory system after the vector (triatomine insect) defecates in a superficial skin wound. Once in the bloodstream, the parasite enters red blood cells (RBCs), white blood cells (WBCs) or platelets, where the next development stage (*amastigote*) begins and the parasite reproduces [37].

After infection, the parasite at the *trypomastigote* stage can be easily differentiated from blood cells. For instance, RBCs have a diameter between 6.2 and 8.2 μm and a thickness between 0.8 and 1 μm [38], while the parasite has a length between 15 and 24 μm [39] and a width of

Name	Test category	Use in laboratory	Detection	State	Sample volume (μL)	Test duration (h.min)	Cost/ test (USD)
Chagas Biosense (BIOTROP)	Rapid assays	No	Direct detection of the parasity Trypanosoma cruzi by microfluidics	Acute	5	0.05	10.83
Chagas STAT-PAK® (Chembio Diagnostic Systems, Inc.)		No	Detection of antibodies for Trypanosoma cruzi by immunochromatographic assay	Chronic	10	0.20	—
HBK 740 IMUNOBLOT LINHAS anti-T. cruzi (Innogenetics, Belgium)	Confirmatory assays	Yes	Indirect immunofluorescence antibody detection		10	1.50	0.19
IMUNOCRUZI® (biolab-Merieux S.A.)		No	Detection of antibodies by immunoblot assay		10	18.00	20
TESA-blot (biolab-Merieux S.A.)		Yes	Detection of antibodies by Western blot		10	4.00	—
CHAGAS HAI IMUNOSERUM (Laboratorio Lemos – Polychaco)	Agglutination	No	Detection of specific antibodies in the sample by hemagglutination		10	1.50	0.33
CHAGAS-ELISA (EBRAM Productos Laboratoriais Ltda)	Enzyme immunoassays	No	Detection of antibodies in the sample by ELISA test		10	1.40	1.02

Table 6. Compared analysis between Chagas biosense and some methods evaluated by the WHO.

approximately 1.09 μm [40]. These differences in size and density suggest the possibility of using a microfluidic device as a separation platform.

Microfluidic devices have already been used in the detection of diseases such as malaria, HIV, and tuberculosis. For example, the detection of HIV is attained by counting the number of CD4 + T-lymphocytes cells in a blood sample, based on the fact that HIV leads to an increase in cell concentration (to levels above 200 cells/mL) [41]. In the case of malaria, the parasite enters RBCs and changes their weight and density, allowing their separation from healthy cells by means of centripetal force [41].

4.2. *In silico* design

4.2.1. Microfluidics fundamentals

Fluid mechanics under the confinement of a microsystem differs from that at the macroscale. For instance, parameters like viscosity, diffusion, adhesion forces and density become significant, while gravity loses strength at the microscale [42]. One of the most important parameters in microfluidics is the Reynolds number (Re), which can be estimated by the following equation:

$$Re = \frac{\rho v D_h}{\mu} \tag{1}$$

Where ρ is the density of the fluid, μ is the viscosity of the fluid, v the velocity of the fluid, and D_h is the hydraulic diameter [43]. The Re can be understood as the ratio of inertial forces to viscous forces [43]. In microfluidics, typical values of Re oscillate around 1, which correspond to the laminar flow regime where viscous forces dominate [42, 44]. In addition, microfluidic devices operating at low Re number can be used for particle separation in a predictable manner [44].

When particles are immersed in a fluid flowing in a microchannel, they are subjected to the Lift force (F_L), which drives them towards zones of higher shear stress [44]. The Lift force can be calculated with the following equation:

$$F_L = \rho G^2 C_L a_p^4 \tag{2}$$

where G is the shear rate of the fluid and is given by $G = v/D_h$, C_L is the lift coefficient, which is a function of the particle position in the channel, and a_p is the diameter of the particle [44].

Particles are also subjected to a secondary force known as the Drag force (F_D). This force is generated by the curvature of the geometry leading to particle trajectories perpendicular to the main flow direction [44]. The Drag force can be evaluated from the following equation:

$$F_D = 5.4{*}10^{-4}\pi\mu De^{1.63}a_p; \;\; De = Re\sqrt{\frac{D_h}{2R}} \tag{3}$$

where De is the Dean number, which describes the effect of curvature in flow nature, and R is the radius of curvature.

As these two forces counterbalance along the microchannel, particle separation is promoted as a strong function of the particle diameter [45]. Thus, the relationship between a_p, F_L and F_D is given by the following set of inequalities, which state that for particles with a large diameter, the dominant force will be F_L. By contrast, if the particle has a small diameter, the dominant force will be F_D.

$$a_{p1} > a_{p2} > a_{p3}; \quad \frac{F_{L1}}{F_{D1}} > \frac{F_{L2}}{F_{D2}} > \frac{F_{L3}}{F_{D3}} \tag{4}$$

4.2.2. Simulations

Prior to microchannel fabrication, particle separation was evaluated *in silico* with the aid of COMSOL Multiphysics®. This tool allowed us to test different microchannel curvatures, diameters and lengths. To set up the simulations, the Computational Fluid Dynamics (CFD) and particle tracing modules were coupled to study the separation of parasites from RBCs for different microchannel configurations. A non-slip condition was defined at the boundaries. **Figure 6** shows the tested design, which consisted of 5 turns of a 0.5 mm wide microchannel that ended up in 4 outlets.

Proper meshing was determined from a mesh convergence analysis by evaluating the magnitude of flow velocity at different locations within the domain. Convergence was met when there was

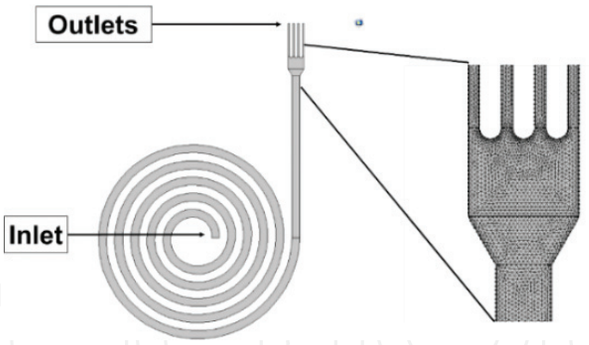

Figure 6. Computational domain and meshing.

less than 2% change on the magnitude of the velocity at each location after duplicating the number of mesh elements in the domain [46]. The parameters for the simulations are listed in **Table 7**:

Fluid density	1030 (Kg/m^3)
Fluid dynamic viscosity	1.5×10^{-3} (Pa s)
Input velocity	0.1 (m/s)
Parasite density	1030 (Kg/m^3)
Parasite diameter	30 (μm)
RBCs density	1030 (Kg/m^3)
RBCs diameter	6 (μm)

Table 7. Simulation parameters.

4.3. Prototypes fabrication

Different manufacturing strategies were used to fabricate the device prototype. These strategies were classified into chemical etching and physical treatments strategies and are described in the following sections.

4.3.1. Chemical etching: photolithography

Chemical etching is a process in which microstructures are generated by the chemical abrasion of a material. Through this process, microstructures can be fabricated on a glass substrate by using hydrofluoric acid (HF) as the etching agent [47]. The protocol for manufacturing the prototype is shown in **Figure 7a**. Briefly, a photoresist layer was spin coated onto a glass slide prior to photolithography (**Figure 7a**). The glass slide was then exposed to HF for 15 seconds to obtain the microchannel. PDMS was adhered to the glass via oxygen plasma irradiation, and served as a sealing layer (**Figure 7a**).

4.3.2. Physical treatment: laser engraving and cutting

Laser engraving and cutting were used as physical techniques for the fabrication of the prototype onto a PMMA substrate. The overall manufacturing process is shown in **Figure 7b**.

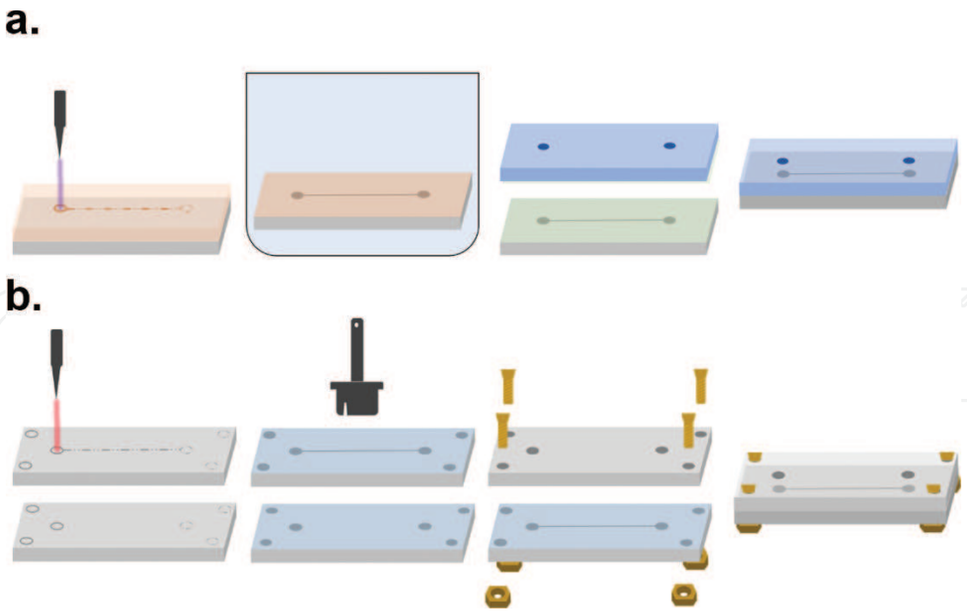

Figure 7. Manufacturing process of biomicrosystems. (**a**) Chemical etching process, and (**b**) laser engraving and cutting.

In brief, the design was engraved into PMMA with a laser cutter (TROTEC® Speedy 100, 60 w). Sealing of the microchannel was attained by application of methyl methacrylate and constant pressure between the layers.

4.4. Results

Currently, the described device is at a design stage. Accordingly, parasite separation has been mainly tested in silico with the aid of the Multiphysics simulation platform COMSOL®. Nonetheless, simulations have given us important insights to be taken into account for preparing more robust prototypes

4.4.1. Simulations

Convergence was attained with 150,000 triangular mesh elements (**Figure 8**). Velocity profiles and particle distributions at the outlets are shown in **Figures 9** and **10**, respectively.

Maximal separation of parasites from RBCs was evidenced in outlets 1 and 3. Nonetheless, there is still a percentage of cross-contamination at the outlets (approximately 25% per outlet). This could be overcome by changing the length of the microchannel or increasing the number of outlets.

4.4.2. Prototypes and proof-of-concept

Functionality and proper sealing of prototypes was tested with water as flowing fluid. Syringes were connected at the inlets through MEDEX® fr 6 urethral nelaton catheters. A Touch Screen (Cole-Parmer®, USA) syringe pump was used to control water flow. Laser engraved prototypes showed leaks when subjected to pressure. In addition, their microchannels dimensions doubled those expected since the manufacturing technique had a low precision in micrometric scales. Furthermore, in the chemical etched prototype, fluid flow was restricted

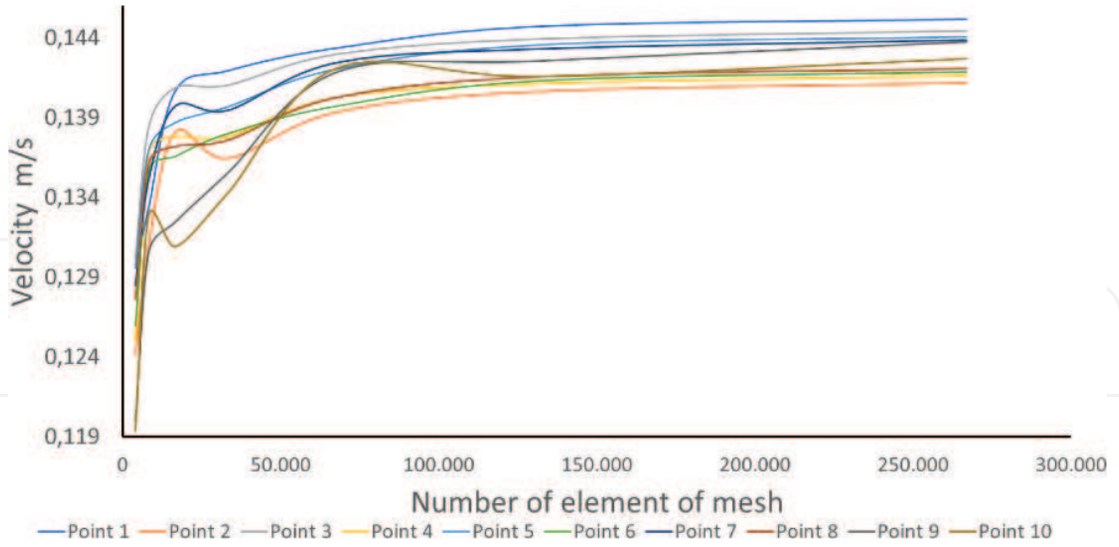

Figure 8. Mesh convergence analysis.

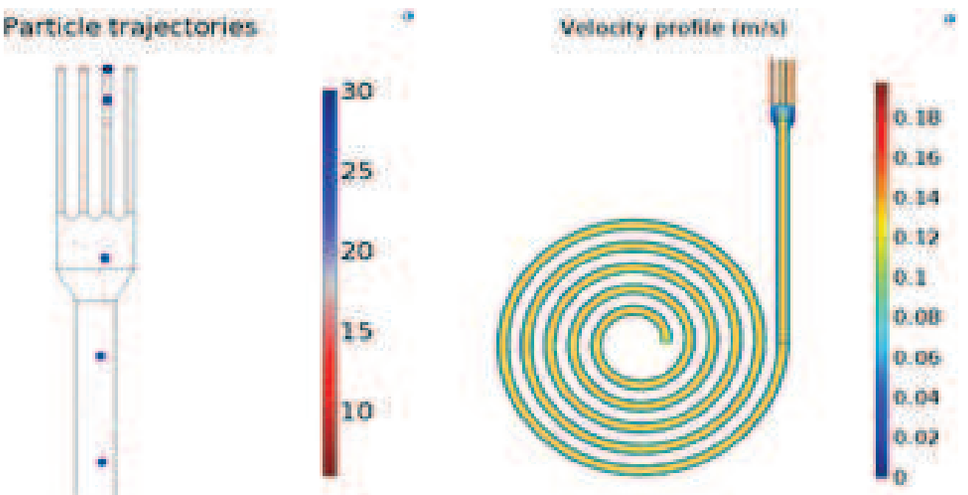

Figure 9. Particle distribution and velocity profile obtained in COMSOL Multiphysics®.

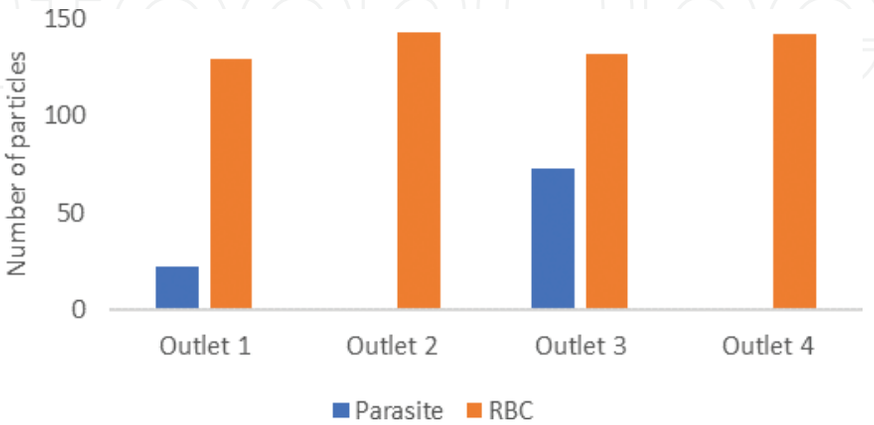

Figure 10. Particle distribution per outlet when simulating 600 particles (100 parasite particles and 500 RBCs particles).

due to the high hydraulic resistance inside the microsystem. To overcome these issues, several strategies can be implemented including a push-in fitting at the inlets to minimize leakages; improved adhesion processes at the interfaces and etched channels with larger dimensions.

4.5. Cost analysis

4.5.1. Disease cost and impact of the device

According to Lee et al. [48], the worldwide expenditure on Chagas Disease is estimated to lay between $186′282,994 and $1638′807,623 USD. 78.35% of which correspond to Latin-America while 18.6% are from the United States and Canada. These costs are principally derived from the treatment of cardiac and digestive complications associated with the disease during the Chronic phase. This roughly represents expenditures of $5900 USD per patient. By contrast, the costs during the Acute phase represent only a single expenditure of $200 USD per patient, which makes diagnosis for the Acute phase the best strategy to reduce the economic burden of treatments on the health care system [49].

The proposed microfluidic system serves as a portable diagnostic device that eliminates the need to attend to specialized laboratories to obtain a diagnosis. This allows rural populations at endemic areas to have a prompt knowledge of their state of health regarding the presence of the Chagas parasite. Also, being able to obtain a diagnosis during the Acute phase will help government agencies to assess the real number of Chagas disease cases, which will result in better awareness and additional research funding.

The expenditure per test of diagnosis varies depending on the stage of the disease. As depicted in **Table 5**, most of the procedures for Chronic phase diagnosis have an approximate cost of $1 USD per test. However, some of the commercially available tests such as the HBK 740 IMUNOBLOT LINHAS anti-T cruzi could have a cost as high as $20 USD per individual test [37]. By contrast, blood testing for Acute phase diagnosis has an approximate cost of $17 USD per patient (Tauramena local Hospital, Colombia).

The Acute phase diagnostic device proposed in this section has an approximate cost of $8 and $4 USD if manufactured via chemical or physical processes, respectively. These costs correspond to expenditures on materials and equipment. In addition to low manufacturing costs, this device does not require specialized laboratory equipment for the diagnosis, allowing its use at remote rural areas, which are usually endemic areas as well.

4.5.2. Future perspectives

Although geometries were verified by simulation processes, there is still a gap between simulated geometries and manufactured prototypes. Sealing techniques must be improved to avoid leaks and increase the life of the device. Also, the microfluidic separation device needs to be coupled with sensing techniques to unequivocally identify the parasite. This could be achieved by including specific antibodies towards *Trypanosoma cruzi* or by placing electrodes at the outlets to determine effective separation by electrical measurements such as electrochemical impedance spectroscopy (EIS).

5. Concluding remarks and future perspectives

Point-of-care devices are ideal for providing reliable information in a fast, user-friendly, accurate, and low-cost manner. Electro-immunosensors offer an attractive option for pathogen detection with high sensitivity and affinity, which can ultimately respond to the challenge of bringing electrochemical sensing techniques to patients. Also, microfluidic separators provide an avenue for isolating and rapidly estimating the relative abundance of pathogens in biological fluids. Rapid diagnosis devices such as those introduced here facilitate clinical decision making and effective treatment thereby leading to greater patient survival rates. The presented case studies show examples in which LoC technology is exploited for pathogen detection. Although the devices show promising results towards early diagnosis of HPV, Tuberculosis and Chagas disease, further work is still needed to bring the developments to commercial success. For instance, the possibility of effectively handling information by end users should be included in the proposed technologies as well as their integration with internet of things (IoT) and cloud computing technology. Also, manufacturing methods that involve drilling can be easily substituted with injection technology, which may reduce costs and time of production. Point-of-care devices constitute the ideal direction towards providing a reliable diagnosis in remote areas without the need of a specialized laboratories or clinical facilities.

Author details

Natalia Lopez-Barbosa[1,2], Ana Lucia Campaña[1,2], Mabel Juliana Noguera[2], Sergio Leonardo Florez[2], Miguel Angel Aroca[1], Juan C. Cruz[2] and Johann F. Osma[1]*

*Address all correspondence to: jf.osma43@uniandes.edu.co

1 CMUA, Department of Electrical and Electronics Engineering, Universidad de los Andes, Bogota, Colombia

2 Department of Biomedical Engineering, Universidad de los Andes, Bogota, Colombia

References

[1] Hay SI, Battle KE, Pigott DM, Smith DL, Moyes CL, Bhatt S, Brownstein JS, Collier N, Myers MF, George DB, Gething PW. Global mapping of infectious disease. Philosophical Transactions of the Royal Society B. 2013;**368**:1-11

[2] Su W, Gao X, Jiang L, Qin J. Microfluidic platform towards point-of-care diagnostics in infectious diseases. Journal of Chromatography. A. 2015;**1377**:13-26. DOI: 10.1016/j.chroma.2014.12.041

[3] Urdea M, Penny LA, Olmsted SS, Giovanni MY, Kaspar P, Shepherd A, Wilson P, Dahl CA, Buchsbaum S, Moeller G, Hay Burgess DC. Requirements for high impact diagnostics in the developing world. Nature. 2006;**444**:73-79

[4] Lopez-Barbosa N, Gamarra JD, Osma JF. The future point-of-care detection of disease and its data capture and handling. Analytical and Bioanalytical Chemistry; 2016. DOI: 10.1007/s00216-015-9249-2

[5] Lopez-Barbosa N, Osma JF. Biosensors: Migrating from clinical to environmental industries. Biosensors Journal. 2016;**5**:1

[6] Wang J. Electrochemical glucose biosensors. Chemical Reviews. 2008;**108**:814-825. DOI: 10.1021/cr068123a

[7] Lopez-Barbosa N, Segura C, Osma JF. Electro-immuno sensors: Current developments and future trends. International Journal Biosensors and Bioelectronics. 2017;**2**:1-6. DOI: 10.15406/ijbsbe.2017.02.00010

[8] Dunne EF, Park IU. HPV and HPV-associated diseases. Infectious Disease Clinics. 2013;**27**: 765-778

[9] Jemal A, Clegg LX, Ward E, Ries LAG, Wu X, Jamison PM, Wingo PA, Howe HL, Anderson RN, Edwards BK. Annual report to the nation on the status of cancer, 1975–2001, with a special feature regarding survival. Cancer. 2004;**101**:3-27

[10] Stanley M. Pathology and epidemiology of HPV infection in females. Gynecologic Oncology. 2010;**117**:S5-S10

[11] Ferlay J, Shin H, Bray F, Forman D, Mathers C, Parkin DM. Estimates of worldwide burden of cancer in 2008: GLOBOCAN 2008. International Journal of Cancer. 2010;**127**:2893-2917

[12] Kornya L, Cseh I, Deak J, Bak M, Fulop V. The diagnostics and prevalence of genital human papillomavirus (HPV) infection in Hungary. European Journal of Obstetrics, Gynecology, and Reproductive Biology. 2002;**100**:231-236

[13] Kim HH, Jeon HJ, Cho HK, Cheong JH, Moon HS, Go JS. Highly sensitive microcantilever biosensors with enhanced sensitivity for detection of human papilloma virus infection. Sensors and Actuators B: Chemical. 2015;**221**:1372-1383

[14] Huang H, Bai W, Dong C, Guo R, Liu Z. An ultrasensitive electrochemical DNA biosensor based on graphene/Au nanorod/polythionine for human papillomavirus DNA detection. Biosensors & Bioelectronics. 2015;**68**:442-446

[15] Urrego LF, Lopez DI, Ramirez KA, Ramirez C, Osma JF. Biomicrosystem design and fabrication for the human papilloma virus 16 detection. Sensors and Actuators B: Chemical. 2015;**207**:97-104. DOI: 10.1016/j.snb.2014.10.036

[16] Saaty TL. Decision making with the analytic hierarchy process. International Journal of Service Science. 2008;**1**:83-98

[17] He F, Xiong Y, Liu J, Tong F, Yan D. Construction of Au-IDE/CFP10-ESAT6 aptamer/DNA-AuNPs MSPQC for rapid detection of *Mycobacterium tuberculosis*. Biosensors & Bioelectronics. 2016;**77**:799-804. DOI: 10.1016/j.bios.2015.10.054

[18] Abe C, Hirano K, Wada M, Kazumi Y, Takahashi M, Fukasawa Y, Yoshimura T, Miyagi C, Goto S. Detection of *Mycobacterium tuberculosis* in clinical specimens by polymerase

chain reaction and gen-probe amplified mycobacterium tuberculosis direct test. Journal of Clinical Microbiology. 1993;**31**:3270-3274

[19] Nassau E, Parsons ER, Johnson GD. The detection of antibodies to *Mycobacterium tuberculosis* by microplate enzyme-linked immunosorbent assay (ELISA). Tubercle. 1976;**57**: 67-70. DOI: 10.1016/0041-3879(76)90019-2

[20] Pottumarthy S, Wells VC, Morris AJ. A comparison of seven tests for serological diagnosis of tuberculosis. Journal of Clinical Microbiology. 2000;**38**:2227-2231

[21] World Health Organization. The End TB Strategy: Global Strategy and Targets for Tuberculosis Prevention, Care and Control After 2015; 2014

[22] Zhang QD, March G, Noel V, Piro B, Reisberg S, Tran LD, Hai LV, Abadia E, Nielsen PE, Sola C, Pham MC. Label-free and reagentless electrochemical detection of PCR fragments using self-assembled quinone derivative monolayer: Application to *Mycobacterium tuberculosis*. Biosensors & Bioelectronics. 2012;**32**:163-168. DOI: 10.1016/j.bios.2011. 11.048

[23] Cheon SA, Cho HH, Kim J, Lee J, Kim HJ, Park TJ. Recent tuberculosis diagnosis toward the end TB strategy. Journal of Microbiological Methods. 2016;**123**:51-61. DOI: 10.1016/j.mimet.2016.02.007

[24] Kim J, Lee K-S, Kim EB, Paik S, Chang CL, Park TJ, Kim H-J, Lee J. Early detection of the growth of *Mycobacterium tuberculosis* using magnetophoretic immunoassay in liquid culture. Biosensors & Bioelectronics. 2017;**96**:68-76. DOI: 10.1016/j.bios.2017.04.025

[25] Costa MP, Andrade CAS, Montenegro RA, Melo FL, Oliveira MDL. Self-assembled monolayers of mercaptobenzoic acid and magnetite nanoparticles as an efficient support for development of tuberculosis genosensor. Journal of Colloid and Interface Science. 2014;**433**:141-148. DOI: http://dx.doi.org/10.1016/j.jcis.2014.07.014

[26] Singh A, Pasha SK, Manickam P, Bhansali S. Single-domain antibody based thermally stable electrochemical immunosensor. Biosensors & Bioelectronics. 2016;**83**:162-168. DOI: 10.1016/j.bios.2016.04.054

[27] Daniels JS, Pourmand N. Label-free impedance biosensors: Opportunities and challenges. Electroanalysis. 2007;**19**:1239-1257. DOI: 10.1002/elan.200603855

[28] Sreejit G, Ahmed A, Parveen N, Jha V, Valluri VL, Ghosh S, Mukhopadhyay S. The ESAT-6 protein of *Mycobacterium tuberculosis* interacts with beta-2-microglobulin (β2M) affecting antigen presentation function of macrophage. PLoS Pathogens. 2014;**10**:e1004446. DOI: 10.1371/journal.ppat.1004446

[29] Sepulveda D, Aroca MA, Varela A, Del Portillo P, Osma JF. Bioelectrochemical detection of *Mycobacterium tuberculosis* ESAT-6 in an antibody-based biomicrosystem. Sensors. 2017;**17**:2178

[30] Technologies A. Agilent 4294A precision impedance analyzer: Operation manual. TEST. 2003;**7**:30-42, 64-78, 130-138

[31] Hotez PJ, Pecoul B, Rijal S, Boehme C, Aksoy S, Malecela M, Tapia-Conyer R, Reeder JC. Eliminating the neglected tropical diseases: Translational science and new technologies. PLoS Neglected Tropical Diseases. 2016;**10**:e0003895

[32] WHO Chagas disease (American trypanosomiasis). http://www.who.int/mediacentre/factsheets/fs340/en/. [Accessed: 12 Sep 2017]; 2017

[33] Capinera JL. Encyclopedia of Entomology. Heidelberg, Germany: Springer Science & Business Media; 2008

[34] Social M de la protección. Protocolo para la vigilancia en salud pública de chagas. Bogotá; 2004

[35] WHO Control of Chagas disease: second report of the WHO expert committee

[36] Abcam Anti-Chagas IgG ELISA Kit (ab178637). http://www.abcam.com/chagas-igg-elisa-kit-ab178637.html. [Accessed 12 Sep 2017]; 2017

[37] Prevention C for DC and DPDx - Laboratory Identification of Parasitic Diseases of Public Health Concern. https://www.cdc.gov/dpdx/. [Accessed 12 Sep 2017]; 2017

[38] Turgeon ML. Clinical Hematology: Theory and Procedures. Philadelphia, USA: Lippincott Williams & Wilkins; 2005

[39] Parasitology TAS for Trypanosoma. http://parasite.org.au/para-site/text/cruzi-text.html. [Accessed 12 Sep 2017]; 2010

[40] Navarro MC, De Lima AR, Askue J, Contreras VT. Morphological comparison of axenic amastigogenesis of trypomastigotes and metacyclic forms of Trypanosoma cruzi. Memórias do Instituto Oswaldo Cruz. 2003;**98**:83-91

[41] Lee WG, Kim Y-G, Chung BG, Demirci U, Khademhosseini A. Nano/microfluidics for diagnosis of infectious diseases in developing countries. Advanced Drug Delivery Reviews. 2010;**62**:449-457

[42] Dimaki M, Okkels F. Design and simulation of lab-on-a-chip devices. In: Lab-on-a-Chip Devices Micro-Total Anal. Syst. Springer International Publishing. Cham, Switzerland; 2015. pp. 27-51

[43] Roselli RJ, Diller KR. Shell balance approach for one-dimensional biofluid transport. In: Biotransport Princ. New York, NY: Appl. Springer New York; 2011. pp. 319-388

[44] Martel JM, Toner M. Inertial focusing in microfluidics. Annual Review of Biomedical Engineering. 2014;**16**:371-396. DOI: 10.1146/annurev-bioeng-121813-120704

[45] Kuntaegowdanahalli SS, Bhagat AAS, Kumar G, Papautsky I, Quake SR, Scrivens WA, Kim KS. Inertial microfluidics for continuous particle separation in spiral microchannels. Lab on a Chip. 2009;**9**:2973. DOI: 10.1039/b908271a

[46] Datta A, Rakesh V. An Introduction to Modeling of Transport Processes: Applications to Biomedical Systems. Cambridge, UK: Cambridge University Press; 2010

[47] Madelung O. Numerical data and functional relationships in science and technology. Landolt Bornstein, New Series, Group III. 1982;**22**:117

[48] Lee BY, Bacon KM, Bottazzi ME, Hotez PJ. Global economic burden of Chagas disease: A computational simulation model. The Lancet Infectious Diseases. 2013;**13**:342-348

[49] Ramsey JM, Elizondo-Cano M, Sanchez-González G, Peña-Nieves A, Figueroa-Lara A. Opportunity cost for early treatment of Chagas disease in Mexico. PLoS Neglected Tropical Diseases. 2014;**8**:e2776

IntechOpen